PNAS RESEARCH ARTICLE | NEUROSCIENCE

Cochlear zinc signaling dysregulation is associated with noise-induced hearing loss, and zinc chelation enhances cochlear recovery

Brandon Bizup[a,b], Sofie Brutsaert[a], Christopher L. Cunningham[a,b,1], Amantha Thathiah[b,1], and Thanos Tzounopoulos[a,b,1]

Edited by Richard Palmiter, University of Washington School of Medicine, Seattle, WA; received June 22, 2023; accepted January 8, 2024

Exposure to loud noise triggers sensory organ damage and degeneration that, in turn, leads to hearing loss. Despite the troublesome impact of noise-induced hearing loss (NIHL) in individuals and societies, treatment strategies that protect and restore hearing are few and insufficient. As such, identification and mechanistic understanding of the signaling pathways involved in NIHL are required. Biological zinc is mostly bound to proteins, where it plays major structural or catalytic roles; however, there is also a pool of unbound, mobile (labile) zinc. Labile zinc is mostly found in vesicles in secretory tissues, where it is released and plays a critical signaling role. In the brain, labile zinc fine-tunes neurotransmission and sensory processing. However, injury-induced dysregulation of labile zinc signaling contributes to neurodegeneration. Here, we tested whether zinc dysregulation occurs and contributes to NIHL in mice. We found that ZnT3, the vesicular zinc transporter responsible for loading zinc into vesicles, is expressed in cochlear hair cells and the spiral limbus, with labile zinc also present in the same areas. Soon after noise trauma, ZnT3 and zinc levels are significantly increased, and their subcellular localization is vastly altered. Disruption of zinc signaling, either via ZnT3 deletion or pharmacological zinc chelation, mitigated NIHL, as evidenced by enhanced auditory brainstem responses, distortion product otoacoustic emissions, and number of hair cell synapses. These data reveal that noise-induced zinc dysregulation is associated with cochlear dysfunction and recovery after NIHL, and point to zinc chelation as a potential treatment for mitigating NIHL.

noise-induced hearing loss | cochlea | zinc | recovery | degeneration

Significance

Labile, not protein-bound, zinc is a powerful neuromodulator in the brain that fine-tunes neurotransmission and sensory processing. However, trauma-induced dysregulation of labile zinc may promote cellular damage and degeneration. Here, we investigated the role of zinc signaling on noise-induced hearing loss (NIHL). We found cell type– and region-specific zinc signaling in the cochlea, which is dysregulated following noise exposure. Genetic or pharmacological disruption of zinc signaling promotes cochlear recovery after noise trauma. As such, these findings highlight that noise-induced zinc dysregulation promotes NIHL and zinc chelators are a potential preventive treatment for mitigating NIHL.

Exposure to loud noise (NE) induces noise-induced hearing loss (NIHL), mainly due to cochlear damage and degeneration (1). In the United States, it is estimated that 17% of adults have NIHL (2, 3). Hearing loss creates substantial deficits in the ability to communicate with the outside world resulting in higher rates of social stress, depression, and injury (4, 5). Data from the 2019 Global Burden of Disease concluded that the total global economic costs of hearing loss exceeded 900 billion USD (5). Despite the high prevalence and the social and economic burden of NIHL, the precise signaling molecules and pathways that can be targeted to prevent, mitigate, or reverse NIHL remain unknown.

Exposure to different durations and intensities of traumatic noise have revealed different types of damage at different cochlear cell types. For example, NE for 2 h at 116 dB SPL or blast exposure causes the loss of hair and supporting cells in the mouse cochlea, as well as shearing of the basilar membrane (1, 6–8). In contrast, "milder" NE (2 h at 98 dB SPL) results in the loss of the synapses between inner hair cells and spiral ganglion neurons (known as hidden hearing loss) and is associated with more subtle auditory deficits, such as the inability to hear clearly in noisy environments (1, 9–11). While many terminal events associated with NIHL are known, it remains unclear what specific signaling pathways participate in NIHL and whether these pathways could provide new targets for preventing, mitigating, or reversing NIHL. Here, we examined the associations of zinc signaling with cochlear dysfunction and recovery after NIHL.

Zinc is essential for life. Most zinc (~90%) is protein-bound and has crucial enzymatic and structural roles (12, 13). The remaining ~10% of zinc is in an unbound (labile) state (14) and performs a crucial signaling role (15, 16). In secretory tissues such as the brain, prostate, and pancreas, labile zinc is loaded in vesicles by the vesicular zinc transporter, ZnT3 (17–19), which is encoded by the *Slc30a3* gene (17, 18). *Slc30a3* gene disruption leads to the complete absence of labile zinc in the brain (18). In the brain, ~50% of excitatory synapses in the neocortex contain vesicular zinc, and activity-dependent zinc release from these vesicles modulates neurotransmission and sensory processing (20–28). Moreover, dysregulation of labile (ZnT3-dependent) zinc signaling has been implicated in multiple models of neurodegeneration, including ischemic stroke and optic nerve injury

Author affiliations: [a]Pittsburgh Hearing Research Center, Department of Otolaryngology, University of Pittsburgh, Pittsburgh, PA 15261; and [b]Department of Neurobiology, University of Pittsburgh, Pittsburgh, PA 15261

Author contributions: B.B., C.L.C., A.T., and T.T. designed research; B.B. and S.B. performed research; B.B. and S.B. analyzed data; and B.B., C.L.C., A.T., and T.T. wrote the paper.

The authors declare no competing interest.

This article is a PNAS Direct Submission.

Copyright © 2024 the Author(s). Published by PNAS. This article is distributed under Creative Commons Attribution-NonCommercial-NoDerivatives License 4.0 (CC BY-NC-ND).

[1]To whom correspondence may be addressed. Email: cunningc@pitt.edu, amantha@pitt.edu, or thanos@pitt.edu.

This article contains supporting information online at https://www.pnas.org/lookup/suppl/doi:10.1073/pnas.2310561121/-/DCSupplemental.

Published February 14, 2024.

(29–31). Namely, labile zinc dysregulation contributes to neurodegeneration and limits the regeneration of injured nervous tissue. Moreover, zinc signaling disruption, by either *Slc30a3* gene deletion or zinc chelation, leads to improved recovery (30–32). In spite of the fact that zinc concentrations in the inner ear are the highest of any organ or tissue in the body (33), zinc signaling has not been thoroughly investigated in the cochlea.

To investigate the role of labile zinc in the cochlea after noise trauma and whether its manipulation affects NIHL, we utilized a recently developed transgenic mouse to examine cell type–specific *Slc30a3* gene expression, in combination with zinc autometallography to localize and quantify ZnT3-dependent zinc. Moreover, we developed a hemagglutinin (HA) epitope-tagged ZnT3-HA knock-in mouse to localize and measure changes in cochlear ZnT3 protein in baseline conditions and in response to NE. We observed cell type–specific expression of ZnT3 and labile zinc in the cochlea and robust zinc and ZnT3 dysregulation after NIHL. Importantly, when we disrupted zinc signaling genetically and pharmacologically, and examined the effects of these manipulations on auditory function, we observed a significant reducing effect on the severity of NIHL.

Results

ZnT3 and ZnT3-Dependent Zinc Are Expressed and Localized in Hair Cells and the Spiral Limbus in the Adult Mouse Cochlea. The cochlear expression pattern of ZnT3, encoded by the gene *Slc30a3*, is unknown; and this knowledge is crucial for understanding the role of zinc signaling in NIHL. To determine the patterns of *Slc30a3* gene expression in the adult mouse cochlea, we employed a recently developed, characterized, and validated transgenic mouse that expresses tamoxifen-induced Cre recombinase ($CreER^{T2}$) in *Slc30a3*-expressing cells (referred to as ZnT3-$CreER^{T2}$ mice) (34). We crossed ZnT3-$CreER^{T2}$ mice with a tdTomato reporter line (Ai14) to generate offspring that express tdTomato in *Slc30a3*-expressing cells after tamoxifen injection (ZnT3-$CreER^{T2}$:Ai14 mice, Fig. 1*A*). We treated 6-wk-old ZnT3-$CreER^{T2}$:Ai14 mice with tamoxifen daily for 5 consecutive days, followed by collection and cryosectioning of their cochlea to evaluate tdTomato expression. We observed prominent tdTomato expression in the organ of Corti, the spiral limbus (SL), and sparsely in the spiral ganglion (Fig. 1*A*), consistent with previous RNAseq studies (35–38). To confirm the tamoxifen-dependence and selectivity of the transgenic construct, we evaluated the cochlea from both ZnT3-$CreER^{T2}$:Ai14 mice that were not injected with tamoxifen (*SI Appendix*, Fig. S1*A*) and tamoxifen-injected wild-type (WT):Ai14 mice (*SI Appendix*, Fig. S1*B*). Neither of these mice showed tdTomato fluorescence in the cochlea, supporting the region-specific and tamoxifen-dependent tdTomato expression in *Slc30a3*-expressing cells in the SL, the organ of Corti, and the spiral ganglion.

Next, we examined the cell-type specificity of *Slc30a3* gene expression in the cochlea. In the SL, which is composed of interdental cells and fibrocytes, interdental cells have a defined cytoarchitectural appearance and localization along the ridge of the SL (39, 40). Unfortunately, there are not any well-established antibodies to delineate SL cell types. Nonetheless, we found that tdTomato-positive cells in the SL do not have either the cytoarchitectural appearance or the localization of interdental cells (Fig. 1*A*). Thus, it is likely that the observed tdTomato staining in the SL represents fibrocytes, supporting *Slc30a3* gene expression in SL fibrocytes.

The cochlear spiral ganglion is composed of neuronal cell bodies, glial cells, and endothelial cells (41, 42). To determine whether the scattered *Slc30a3*-expressing tdTomato cells in the spiral ganglion include spiral ganglion neurons (SGNs), we immunostained cryosections from tamoxifen-induced ZnT3-$CreER^{T2}$:Ai14 mice with an antibody against β3-tubulin (Tuj1) to label SGNs and their dendrites and counterstained nuclei with DAPI (Fig. 1 *A*, *Bottom*). We found that tdTomato labeling was not colocalized with Tuj1, suggesting that the *Slc30a3* gene is not expressed in SGNs (Fig. 1*A*). To further confirm that the *Slc30a3* gene is not expressed in SGNs, we immunostained cryosections from tamoxifen-induced ZnT3-$CreER^{T2}$:Ai14 mice with an antibody against neurofilament (NF-H), which is another marker for SGNs. We observed that tdTomato labeling was not colocalized with NF-H immunolabeling

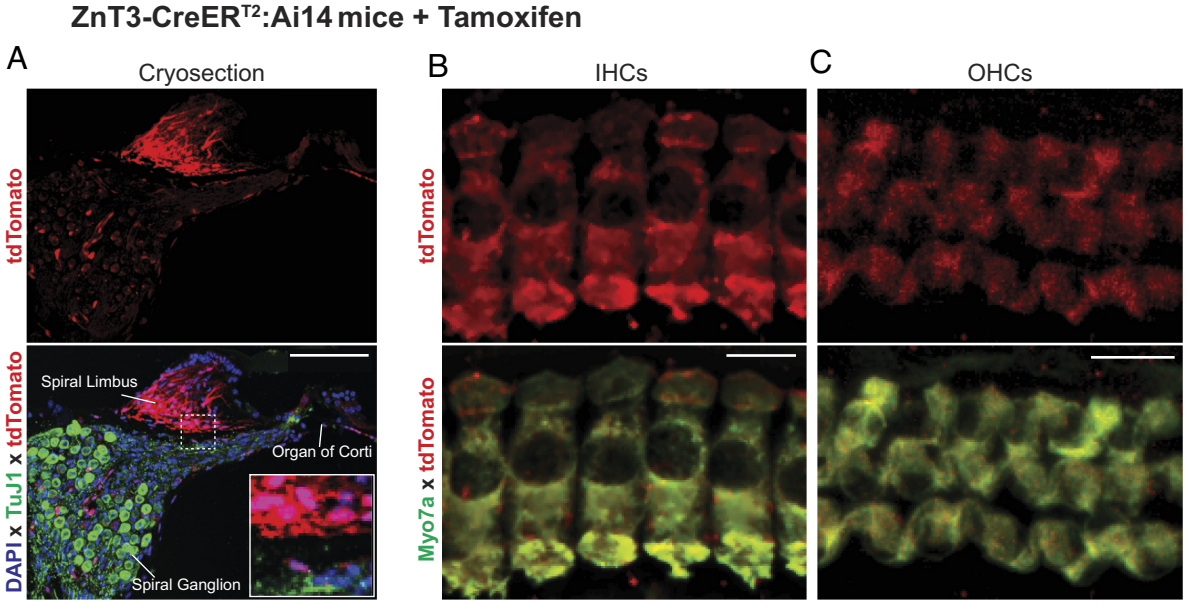

Fig. 1. The *Slc30a3* gene is expressed in the spiral limbus (SL), spiral ganglion, and cochlear IHCs and OHCs. (*A*) Representative image of the midmodiolar cryostat section of ZnT3-$CreER^{T2}$:Ai14 mouse cochleas with tamoxifen induction. Sections are labeled with tdTomato (*Slc30a3* gene expression; red), Tuj1 (SGNs; green), and DAPI (nuclei; blue). (Scale bar: 100 μm.) (*B* and *C*) Representative images of IHCs (*B*) and OHCs (*C*) from cochlear whole mounts of ZnT3-$CreER^{T2}$:Ai14 mice labeled with tdTomato (*Slc30a3* gene expression; red) and Myo7a (hair cells; green). (Scale bar: 10 μm.)

(*SI Appendix*, Fig. S1*C*), confirming that SGNs do not express the *Slc30a3* gene. As such, these results suggest that in the spiral ganglion, the *Slc30a3* gene is likely expressed by a select population of glia or endothelial cells, but not neuronal cells.

The organ of Corti is composed of hair cells and a diverse array of supporting cells (40). To assess cell-type specificity of *Slc30a3* gene expression in the organ of Corti, we used an antibody against Myosin VIIa (Myo7a) to immunolabel hair cells in cochlear whole mounts from tamoxifen-induced ZnT3-CreER^{T2}:Ai14 mice (Fig. 1 *B* and *C*). We found robust tdTomato expression in inner hair cells (IHCs; Fig. 1*B*) and outer hair cells (OHCs; Fig. 1*C*), but not other cell types, consistent with previous transcriptomic studies (37, 38, 43).

Our results from the ZnT3-CreER^{T2}:Ai14 mouse identified cochlear cells that express the *Slc30a3* gene but do not address ZnT3 protein expression patterns (34). To determine ZnT3 protein localization, we initially utilized commercially available antibodies for ZnT3 (*Materials and Methods*). However, none of these antibodies displayed sufficient specificity for cochlea immunolocalization. To overcome this limitation, we developed a knock-in mouse that expresses a human influenza hemagglutinin (HA) epitope tag at the C terminus of the endogenous *Slc30a3* gene (referred to as ZnT3-HA mice). Prior to assessing cochlear ZnT3 expression in the ZnT3-HA mouse, we tested whether the expression pattern of ZnT3-HA was consistent with previous studies in different brain areas where ZnT3 expression and labile zinc distribution are known. We found that the expression pattern and relative levels of ZnT3-HA in the hippocampus and neocortex are consistent with established data on ZnT3 expression and labile zinc concentration and distribution (17, 44, 45) (*SI Appendix*, Fig. S1*D*). Furthermore, to confirm that ZnT3-HA mice accumulate vesicular zinc in the same regions as wild-type (WT) mice, we performed zinc autometallography (also called Timm stain 46) to stain labile zinc in brain slices from ZnT3-HA mice. We observed that labile zinc accumulation in ZnT3-HA mice is similar to the ZnT3-HA expression patterns in ZnT3-HA mice (*SI Appendix*, Fig. S1 *D* and *E*), which is consistent with findings from WT mice (17, 44, 45), thus confirming that ZnT3-HA mice also accumulate labile zinc in the same regions as WT mice. Finally, to control for potential effects of this mouse on cochlear function, we assessed auditory brainstem responses (ABRs) in ZnT3-HA and WT mice. ABR measurements reflect the coordinated electrical activity of the auditory nerve (wave I) and ascending auditory brainstem in response to sounds of varying frequency and intensity (47–49). The ABR threshold is the minimum sound level intensity that evokes an ABR wave I and reflects hearing threshold. ABR thresholds in ZnT3-HA were not different from those in WT (*SI Appendix*, Fig. S1*F*), supporting that tagging ZnT3 with HA did not have any obvious impact on auditory function.

Having validated the ZnT3-HA mouse, we next assessed ZnT3 protein expression in the cochlea. We observed ZnT3-HA expression in the SL and organ of Corti (Fig. 2*A*; parvalbumin, PV, antibody was used to identify hair cells), which is in agreement with our results from ZnT3-CreER^{T2}:Ai14 mice (Fig. 1 *A*–*C*) and transcriptomic studies (37, 38, 43). We did not observe ZnT3-HA expression in the spiral ganglion (*SI Appendix*, Fig. S1*G*), suggesting that the *Slc30a3*-expressing cells observed in ZnT3-CreER^{T2}:Ai14 mice either do not produce ZnT3 protein or produce ZnT3 levels that were below the threshold for detection in our experiments.

To further investigate ZnT3 expression in the organ of Corti, we immunostained cochlear whole mounts from 6-wk-old ZnT3-HA and WT mice. We determined that both IHCs (Fig. 2*B*) and OHCs (Fig. 2*C*) expressed ZnT3-HA. ZnT3-HA expression showed a punctate pattern that was distributed throughout the soma. In the brain, ZnT3 is associated with presynaptic vesicles. To determine whether ZnT3-HA localization in IHCs corresponds to presynaptic ribbon synapses, we labeled presynaptic IHC ribbon synapses with an anti-C-terminal-binding protein 2 antibody (CtBP2). We did not observe any colocalization between ZnT3-HA and CtBP2 (*SI Appendix*, Fig. S1*H*), supporting that ZnT3-HA is not associated with synaptic vesicles in IHCs.

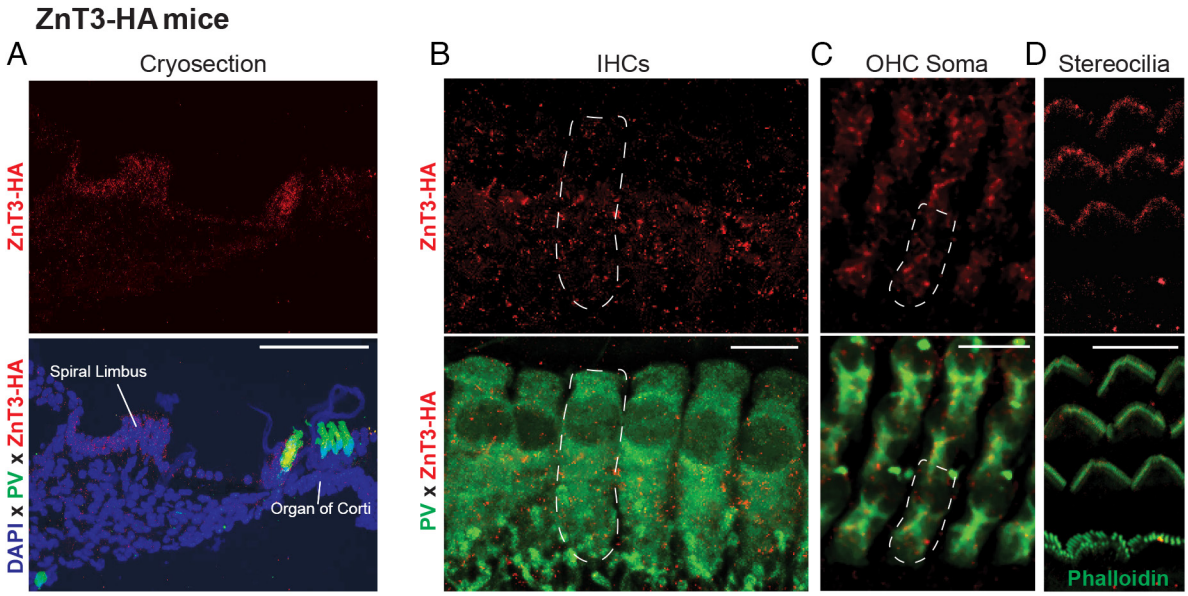

Fig. 2. ZnT3 protein is expressed in the SL and cochlear IHCs and OHCs. (*A*) Representative image of the midmodiolar cryostat section of ZnT3-HA mouse cochleas. Sections are immunolabeled for the HA tag (ZnT3-HA; red) and parvalbumin (hair cells; green), and nuclei are counterstained with DAPI (nuclei; blue). (Scale bar: 100 μm.) (*B* and *C*) Representative images of IHCs (*B*) and OHCs (*C*) from cochlear whole mounts of ZnT3-HA mice immunolabeled for the HA tag (ZnT3-HA; red) and parvalbumin (hair cells; green). (Scale bar: 10 μm.) (*D*) Single plane confocal image of the stereocilia of IHCs and OHCs from cochlear whole mounts of ZnT3-HA mice labeled for the HA tag (ZnT3-HA; red) and dyed with phalloidin (stereocilia; green). (Scale bar: 10 μm.) For all representative images, similar results were obtained in at least three independent samples.

IHCs and OHCs are crowned by actin-rich stereocilia, which are crucial for mechanotransduction of sound (50). By labeling the stereocilia with phalloidin, we observed that ZnT3-HA is also localized to the stereocilia of OHCs, but not IHCs (Fig. 2*D* and *Discussion*). Given that ZnT3 is a transmembrane protein, this result suggests that ZnT3 localizes to the plasma membrane of stereocilia in OHCs. This is in contrast to previous studies in other areas supporting that ZnT3 is typically located on vesicles (45, 51); and to our knowledge, there are no vesicles in hair cell stereocilia (*Discussion*). In WT mice that lack the HA tag, no HA-tag immunolabeling was observed (*SI Appendix*, Fig. S1*I*), supporting the specificity of our experimental approach. Together, these results demonstrate that ZnT3 is expressed in subsets of cells in the cochlea, including IHCs, OHCs, and fibrocytes in the SL.

Next, we addressed where labile zinc resides in the cochlea. In the brain, localization of the mRNA that encodes ZnT3 is consistent with histochemically stained zinc (17, 52). We labeled labile zinc with Timm staining (46) in cochlear whole mounts from wild-type (WT) mice and mice with *Slc30a3* gene deletion (ZnT3-KO), which lack ZnT3 protein and labile zinc (18). Consistent with ZnT3 protein localization, we found that labile zinc is localized to hair cells. In OHCs, labile zinc displays a stereocilia-like pattern and diffuse staining throughout the cell body (Fig. 3*A*). We did not observe any zinc staining in the OHCs of ZnT3-KO mice (Fig. 3*B*). Additionally, zinc staining was observed throughout the cell body of IHCs of WT mice (Fig. 3*C*) and was absent in ZnT3-KO mice (Fig. 3*D*). No obvious stereocilia-like zinc staining pattern was apparent in IHCs. We also observed zinc staining in the SL, which was most prominent in the area adjacent to the inner sulcus that contains fibrocytes (39, 40) (Fig. 3*E*). Labile zinc staining was not detected in the SL of ZnT3-KO mice (Fig. 3*F*). In the spiral ganglion, we did not observe any differences in the Timm staining between WT and ZnT3-KO mice, but we saw signal in the ZnT3-KO spiral ganglion (*SI Appendix*, Fig. S1*J*). Thus, although the similarity between WT and ZnT3-KO mice is consistent with the lack of ZnT3-dependent zinc in this area and the lack of ZnT3 protein in the spiral ganglion (*SI Appendix*, Fig. S1*G*), the Timm signal in the ZnT3-KO mice reduces our confidence in assessing mobile zinc in the spiral ganglion. Taken together, these results indicate that IHC, OHCs, and SL display prominent ZnT3-dependent labile zinc signal, consistent with *Slc30a3* gene and ZnT3 protein expression in these cochlear cell types and areas (Figs. 1 and 2).

Loud Noise Exposure Causes Dysregulation of Labile Zinc and ZnT3 Levels in the Cochlea. Although dysregulated zinc signaling has been implicated in tissue degeneration associated with trauma, such as optic nerve crush (31) and ischemic stroke (29), it is unknown whether zinc signaling is altered and potentially involved in noise trauma-induced cochlear degeneration. To address this question, we bilaterally exposed unanesthetized mice to 100 dB SPL 8 to 16 kHz noise for 2 h (*SI Appendix*, Fig. S2*A*), which causes cochlear damage and hearing threshold shifts, as assessed by ABR measurements at 1 d and 14 d after noise trauma (8, 53, 54) (*SI Appendix*, Fig. S2 *B* and *C*). We then evaluated zinc and ZnT3 levels and localization at different time points after noise trauma. We observed a profound increase and redistribution of zinc in the cochlea (zinc dysregulation), relative to sham-exposed (SE) mice 1 d after NE. Whereas labile zinc was primarily observed in a stereocilia-like arrangement in OHCs of SE-mice (Fig. 4 *A*, *Top*), NE led to a striking increase and redistribution of zinc throughout the cell body of the OHCs (Fig. 4 *A*, *Bottom*, quantified in Fig. 4*B*). Moreover, NE led to a marked increase of zinc in the IHCs relative to SE mice (Fig. 4 *E* and *F*). Finally,

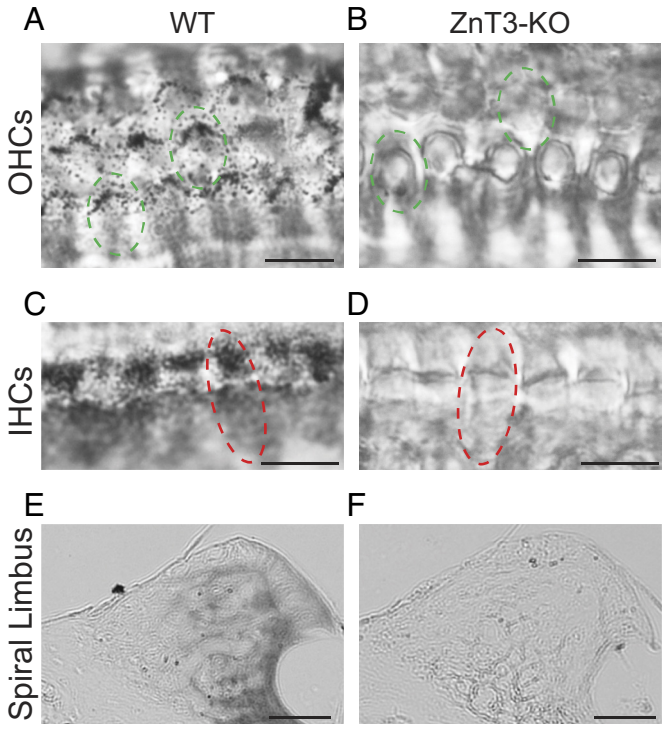

Fig. 3. ZnT3-dependent zinc is present in cochlear OHCs and IHCs and the SL. (*A*) Representative Timm stained cochlear whole mount of the OHC region from the WT mouse. Green circles indicate approximate OHC cell bodies. (Scale bar: 10 μm.) (*B*) Representative Timm stained cochlear whole mount of the OHC region from the ZnT3-KO mouse. Green circles indicate approximate OHC cell bodies. (Scale bar: 10 μm.) (*C*) Representative Timm stained cochlear whole mount of the IHC region from the WT mouse. The red circle indicates approximate IHC cell body. (Scale bar: 10 μm.) (*D*) Representative Timm stained cochlear whole mount of the IHC region from the ZnT3-KO mouse. The red circle indicates approximate IHC cell body. (Scale bar: 10 μm.) (*E*) Representative midmodiolar Timm stained microtome section of the SL region from the WT mouse. (Scale bar: 50 μm.) (*F*) Representative midmodiolar Timm stained microtome section of the SL region from the ZnT3-KO mouse. (Scale bar: 50 μm.) For all representative images, similar results were obtained in at least three independent samples.

NE caused a similar elevation and broader distribution in the SL relative to SE mice (Fig. 4 *I* and *J*). These results support robust mobile zinc dysregulation in hair cells and the SL 1 d after NE.

To determine whether the observed zinc dysregulation is ZnT3-dependent, we investigated the effect of NE on the levels and localization of zinc in ZnT3-KO mice. Consistent with our previous results (Fig. 3), we did not observe any zinc staining in either SE- or NE-mice in either OHCs (*SI Appendix*, Fig. S3*A*), IHCs (*SI Appendix*, Fig. S3*D*), or the SL (*SI Appendix*, Fig. S3*G*). These results support the ZnT3-dependence of the dysregulation of cochlear labile zinc after NE (*Discussion*).

To determine whether noise trauma-induced zinc dysregulation was associated with concurrent changes in ZnT3 protein levels, we immunostained cochlea cryosections and whole mounts from NE ZnT3-HA mice. We observed an increase in ZnT3-HA levels in IHCs (Fig. 4 *C* and *D*), OHCs (Fig. 4 *G* and *H*) and SL (Fig. 4 *K* and *L*) of NE mice relative to SE mice. Consistent with the lack of ZnT3-HA staining in the spiral ganglion in control conditions (*SI Appendix*, Fig. S1*G*), we did not observe any ZnT3-HA staining in the spiral ganglion of ZnT3-HA mice after either SE or NE (*SI Appendix*, Fig. S3*J*). To control for potential effects of the HA tag on ZnT3-dependent zinc distribution, we investigated the localization and noise-induced dysregulation of labile zinc in cochlear whole mounts from ZnT3-HA mice 1 d after SE or NE. We found similar localization and noise-induced dysregulation of

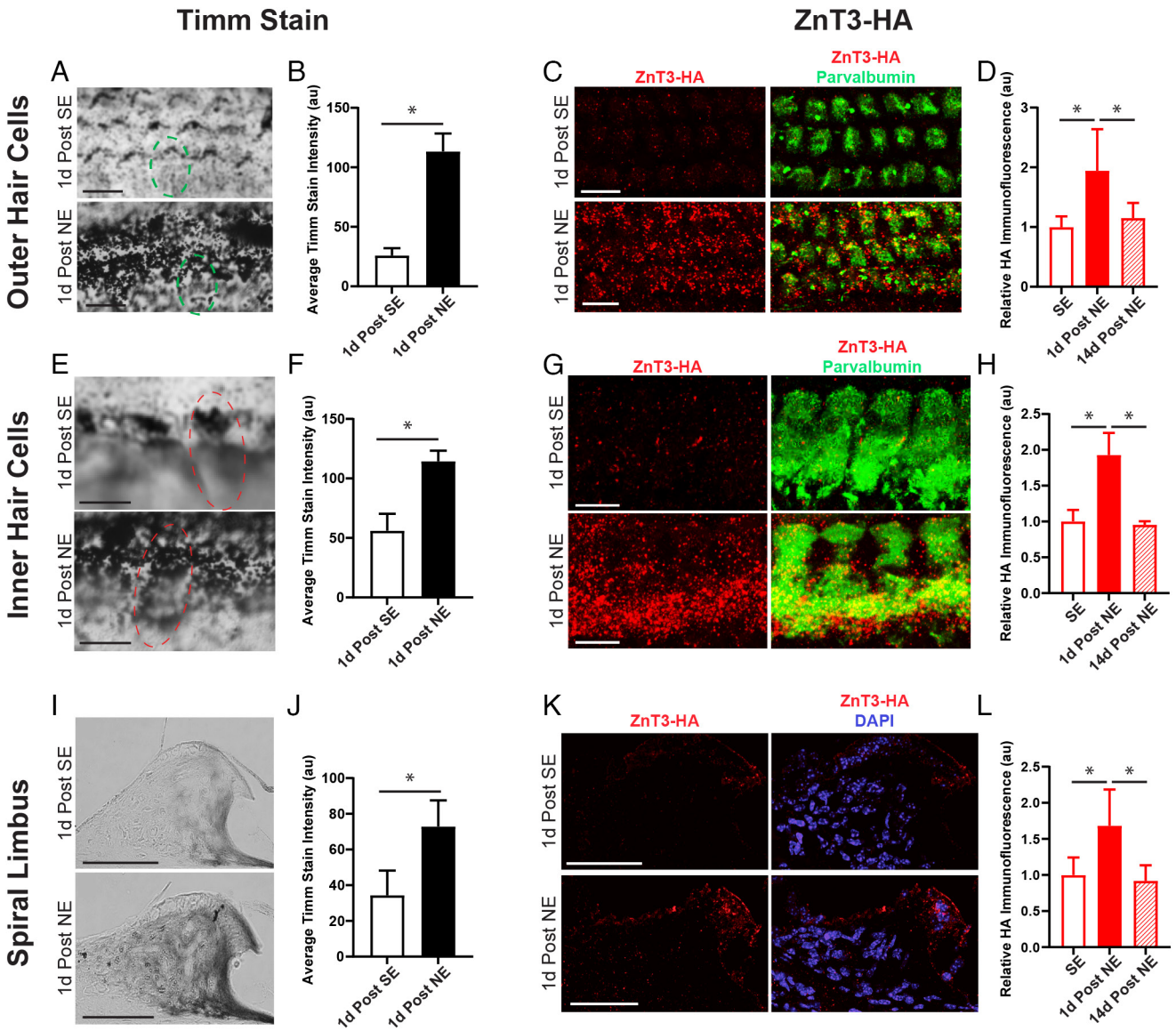

Fig. 4. Noise exposure dysregulates ZnT3 and labile zinc in the cochlea. (*A*) Representative Timm stains from wild-type cochlea whole mount in the OHCs 1 d after SE (*Top*) and NE (*Bottom*). (Scale bar: 10 μm.) (*B*) Quantification of zinc staining in OHC region after SE and NE in WT mice ($P = 0.0004$, n = 3 mice/group). (*C*) Representative image of OHCs from cochlear whole mounts of ZnT3-HA mice 1 d after SE (*Top*) and NE (*Bottom*) showing ZnT3-HA staining (red). Hair cells are labeled with anti-parvalbumin antibody (green). (Scale bar: 10 μm.) (*D*) Quantification of ZnT3-HA immunofluorescence in the OHC region 1 d and 14 d after SE and NE in ZnT3-HA mice (SE vs. 1 d post-NE, $P = 0.0345$; 1 d vs. 14 d, $P = 0.0484$; n = 4 mice/group). (*E*) Representative Timm stains from wild-type cochlea whole mount in the IHCs 1 d after SE (*Top*) and NE (*Bottom*). (Scale bar: 10 μm.) (*F*) Quantification of zinc staining in the OHC region after SE and NE in WT mice ($P = 0.0115$, n = 3 mice/group). (*G*) Representative image of IHCs from cochlear whole mounts of ZnT3-HA mice 1 d after SE (*Top*) and NE (*Bottom*) showing ZnT3-HA staining (red). Hair cells are labeled with anti-parvalbumin antibody (green). (Scale bar: 10 μm.) (*H*) Quantification of ZnT3-HA immunofluorescence in the IHC region 1 d and 14 d after SE and NE in ZnT3-HA mice (SE vs. 1 d, $P = 0.0206$; 1 d vs. 14 d, $P = 0.0332$; n = 4 mice/group). (*I*) Representative Timm stains of the SL region from WT mouse cochlea microtome sections 24 after SE (*Top*) or NE (*Bottom*). (Scale bar: 50 μm.) (*J*) Quantification of zinc staining in SL after SE and NE in WT mice ($P = 0.0075$, SE n = 3, NE n = 4). (*K*) Representative image of ZnT3-HA stains (red) in SL 1 d after SE (*Top*) and NE (*Bottom*). Nuclei are counterstained with DAPI (blue). (Scale bar: 50 μm.) (*L*) Quantification of ZnT3-HA immunofluorescence in SL 1 d and 14 d after SE and NE in ZnT3-HA mice (SE vs. 1 d, $P = 0.0398$; 1 d vs. 14 d, $P = 0.0471$; n = 4 mice/group). Quantified data are shown as mean ± SEM. For statistical details, see *SI Appendix*, Table S1.

labile zinc in IHCs and OHCs, indicating that labile zinc dysregulation in the cochlea is not affected by the HA epitope tag (*SI Appendix*, Fig. S3 *K* and *L*). Together, these results indicate that NE leads to an increase (and dysregulation) in labile zinc and ZnT3 protein levels in hair cells and the SL 1 d after NE and suggest that elevated ZnT3 levels are associated with labile zinc dysregulation in these areas.

To evaluate whether the elevation in ZnT3-HA protein levels persists after NE, we collected and immunostained cochleas from ZnT3-HA mice 14 d after NE. We found that 14 d after NE, ZnT3-HA levels in hair cells (Fig. 4 *D* and *H* and *SI Appendix*, Fig. S3 *C* and *F* for representative images) and the SL (Fig. 4*L* and *SI Appendix*, Fig. S3*I* for representative images) were not different than 14 d after SE, indicating that ZnT3 protein levels return to baseline after the initial increase in expression.

To quantify cochlea-wide changes in native ZnT3 protein levels after NE, we performed western blot analysis on protein samples 1 d after NE or SE in ZnT3-KO and WT mice. We observed two ZnT3-immunoreactive bands in cochleas from WT mice, at 42 kDa and 84 kDa, which are absent in the ZnT3-KO mice (*SI Appendix*, Fig. S4*A*). In NE mice, we observed an increased total amount of cochlear ZnT3 protein levels (*SI Appendix*, Fig. S4 *A* and *B*), which was primarily due to an increase in the intensity of the 84 kDa, but not 42 kDa, ZnT3 band (*SI Appendix*, Fig. S4

C and *D*). The increase in the 84 kDa ZnT3 band is consistent with an increase in ZnT3 dimerization after NE, although we cannot safely conclude that this band represents a ZnT3 dimer (*Discussion*). Taken together, NE causes a profound increase and redistribution of ZnT3-dependent zinc and ZnT3 in the cochlea, both in the organ of Corti and the SL.

ZnT3 Knockout Due to *Slc30a3* Gene Deletion Mitigates NIHL. To investigate whether the trauma-induced dysregulation of zinc signaling contributes to NIHL, we compared ABRs from 6- to 8-wk old WT and ZnT3-KO mice (Fig. 5*A*). We found that neither baseline ABR thresholds nor ABR Wave I amplitudes were different between mice with *Slc30a3* gene deletion (ZnT3-KO) and WT mice (*SI Appendix*, Fig. S5 *A–C*), suggesting that *Slc30a3* gene deletion does not affect hearing thresholds. One day after NE, WT mice displayed elevated ABR thresholds, consistent with previous work (8, 53, 54) (Fig. 5*B*, three-way ANOVA). To evaluate potential effects of *Slc30a3* gene deletion (as frequency had no effect), we averaged threshold shifts across frequencies and used a 2-way ANOVA. We found that *Slc30a3* gene deletion did not affect ABR threshold shifts 1 d after NE (Fig. 5 *B* and *C*). When we evaluated ABR threshold shifts 14 d after NE, we found that ABR threshold shifts were significantly higher in NE than SE mice, demonstrating a long-lasting threshold shift (Fig. 5*D*). To explore the effects of *Slc30a3* gene deletion at 14 d after NE, we averaged threshold shifts across frequencies and found that threshold shifts in ZnT3-KO NE-mice were significantly reduced compared to WT NE-mice (Fig. 5*E*). Because both WT and KO

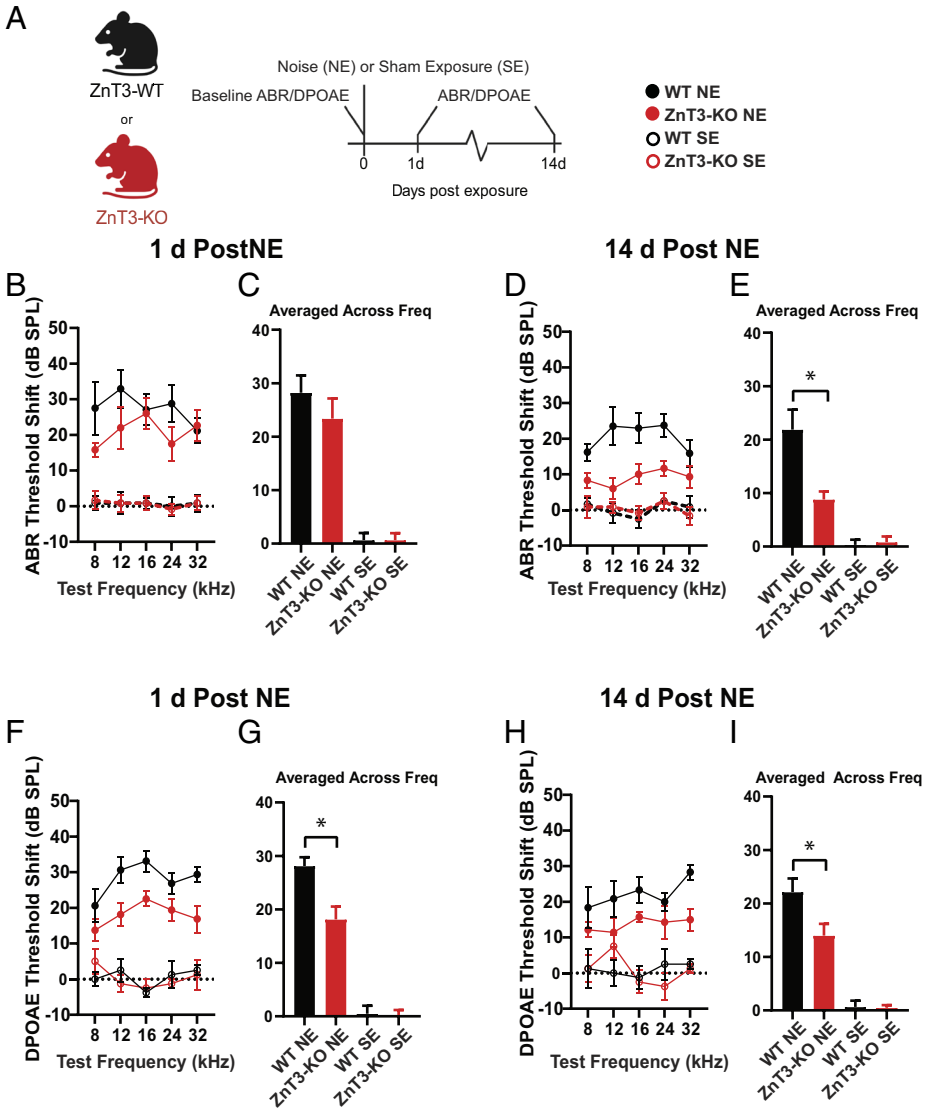

Fig. 5. ZnT3 knockout due to *Slc30a3* gene deletion mitigates cochlear dysfunction after NE. (*A*) Experimental design. Baseline ABRs and DPOAEs were recorded from WT and ZnT3-KO mice prior to SE or NE (100 dB SPL, 8 to 16 kHz for 2 h). ABRs and DPOAEs were again measured 1 d and 14 d post-NE and -SE. (*B*) Average ABR threshold shifts 1 d after NE or SE in WT (black) and ZnT3-KO (red) mice. (n = 17 WT+NE, 15 ZnT3-KO+NE, 6 WT+SE, 6 ZnT3-KO+SE). (*C*) ABR threshold shifts from (*B*) averaged across frequencies 1 d after NE. (Noise × Genotype Interaction $P = 0.5609$; n = 17 WT+NE, 15 ZnT3-KO+NE, 6 WT+SE, 6 ZnT3-KO+SE). (*D*) Average ABR threshold shifts 14 d after NE or SE in WT (black) and ZnT3-KO (red) mice. (n = 17 WT+NE, 15 ZnT3-KO+NE, 6 WT+SE, 6 ZnT3-KO+SE). (*E*) ABR threshold shifts from (*D*) averaged across frequencies 14 d after NE. ZnT3-KO mice ABR threshold shifts are significantly smaller than WT mice after NE (WT+NE vs. ZnT3-KO+NE $*P = 0.0061$; n = 17 WT+NE, 15 ZnT3-KO+NE, 6 WT+SE, 6 ZnT3-KO+SE). (*F*) Average DPOAE threshold shifts 1 d after NE or SE in WT (black) and ZnT3-KO (red) mice. (n = 8 WT+NE, 8 ZnT3-KO+NE, 4 WT+SE, 4 ZnT3-KO+SE). (*G*) DPOAE threshold shifts from (*F*) averaged across frequencies 1 d after NE. ZnT3-KO mice DPOAE threshold shifts are significantly smaller than WT mice after NE (WT+NE vs. ZnT3-KO+NE, $*P = 0.0049$; n = 8 WT+NE, 8 ZnT3-KO+NE, 4 WT+SE, 4 ZnT3-KO+SE). (*H*) Average DPOAE threshold shifts 14 d after NE or SE in WT (black) and ZnT3-KO (red) mice. (n = 8 WT+NE, 9 ZnT3-KO+NE, 6 WT+SE, 6 ZnT3-KO+SE). (*I*) DPOAE threshold shifts from (*H*) averaged across frequencies 14 d after NE. ZnT3-KO mice DPOAE threshold shifts are significantly smaller than WT mice 14 d after NE (WT+NE vs. ZnT3-KO+NE, $*P = 0.0344$; n = 8 WT+NE, 9 ZnT3-KO+NE, 6 WT+SE, 6 ZnT3-KO+SE). Data are shown as mean ± SEM. For statistical details, see *SI Appendix*, Table S1.

mice showed robust, similar threshold shifts 1 d after NE, but ZnT3-KO mice showed reduced threshold shifts compared to WT mice 14 d after NE, these results suggest that *Slc30a3* gene deletion, leading to ZnT3 knockout, does not alter the initial effects of NE (1 d) but likely enhances the recovery (14 d) of cochlear function following NE (*Discussion*).

Consistent with reduced threshold shifts in ZnT3-KO compared to WT mice, we found significantly higher ABR Wave I amplitudes in ZnT3-KO relative to WT mice at both 1 d and 14 d post-NE (*SI Appendix*, Fig. S5 *D* and *E*). Finally, we did not find any difference in the Wave IV/I ratio (gain) between WT and ZnT3-KO mice either before or 1 d after and 14 d after NE, suggesting that changes in brainstem gain in response to NE likely do not contribute to the enhanced recovery of cochlear function following NE in ZnT3-KO mice (*SI Appendix*, Fig. S5 *F–H*).

While ABR threshold shifts assess overall cochlear output via the auditory nerve, distortion product otoacoustic emissions (DPOAEs) are a correlate of OHC health and function (55, 56). DPOAEs refer to the weak sounds that can be recorded from the ear canal in response to stimuli after amplification by OHCs. As such, DPOAEs assess the function of OHCs. We recorded DPOAEs in WT and ZnT3-KO mice (Fig. 5*A*). Baseline DPOAE thresholds were not different between WT and ZnT3-KO mice (*SI Appendix*, Fig. S5 *I* and *J*). One day after NE, both ZnT3-KO and WT mice showed elevated DPOAE thresholds, with no frequency effect (Fig. 5*F*). However, the threshold shift was lower in ZnT3-KO NE-mice at 1 d after NE compared to WT NE-mice, when averaged across frequencies, suggesting that *Slc30a3* gene deletion mitigates the initial, 1 d after noise trauma, damage to OHC function (Fig. 5*G*). Furthermore, we found that DPOAE threshold shifts from ZnT3-KO mice were lower 14 d after NE relative to WT mice (Fig. 5 *H–I*). These results indicate that *Slc30a3* gene deletion mitigates the damage of cochlear OHCs as assessed 1 d after noise trauma and that this protection is consistent with improved OHC function up to 14 d after NE.

ZnT3 Knockout Due to *Slc30a3* Gene Deletion Mitigates Noise-Induced Cochlear Synapse Loss. To investigate the anatomical basis of the protection and enhanced recovery of ABR and DPOAE threshold shifts in ZnT3-KO mice after NE, we performed immunohistochemical analysis of the cochlea from WT and ZnT3-KO mice. We did not observe any loss of IHCs or OHCs along the cochlear frequency axis (8 kHz-32 kHz) in WT or ZnT3-KO mice 1 d or 14 d after NE (*SI Appendix*, Fig. S5 *K–N*), suggesting that the observed threshold shifts are not due to hair cell loss.

NE causes cochlear synapse loss (synaptopathy), i.e., the loss of synapses between IHCs and SGN peripheral axons, known as ribbon synapses (9, 10). Each SGN forms a single ribbon synapse with one IHC (57), and each IHC forms synapses with 5 to 30 SGNs, depending on the location along the cochlear frequency axis. To evaluate whether noise-induced zinc dysregulation contributes to synaptopathy, we quantified ribbon synapse numbers in WT and ZnT3-KO SE- and NE-mice. We labeled presynaptic IHC ribbon synapses with an anti-CtBP2 antibody (Fig. 6 *A–D*) and postsynaptic glutamate AMPA receptors with an anti-GluR2 antibody (GluR2, Fig. 6 *A–D*). We then determined the number of intact ribbon synapses by quantifying the number of adjacent/overlapping CtBP2 and GluR2 puncta in regions of the cochlea that correspond to the tested ABR and DPOAE frequencies, (i.e., 8, 12, 16, 24, and 32 kHz). Cochleas from SE WT and ZnT3-KO mice displayed similar numbers of ribbon synapses per IHC (Fig. 6 *A*, *B*, and *E* open circles), suggesting that *Slc30a3* gene deletion does not affect baseline cochlear synapse density. Consistent with previous studies (9, 10), 1 d after NE, we observed a 50% loss of intact ribbon

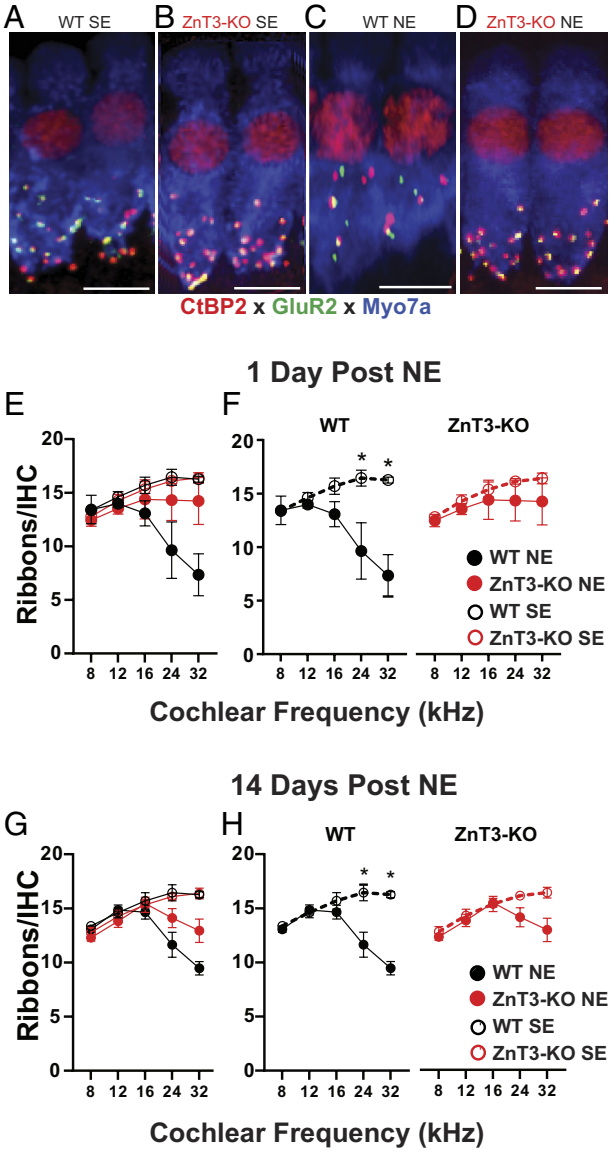

Fig. 6. ZnT3 knockout due to *Slc30a3* gene deletion mitigates noise-induced cochlear synaptopathy. (*A–D*) Representative maximum projection images of cochlear whole mount IHCs from the 32 kHz region of cochleas. Whole mounts are labeled with Myo7a (blue), CtBP2 (red), and GluR2 (green). This staining protocol allows for the identification of IHCs (blue somata with red nuclei) and presynaptic ribbon synapses (red puncta) with their postsynaptic glutamate receptor patches (green puncta). Ribbon synapses are considered intact only when presynaptic red puncta are adjacent to postsynaptic green puncta. (*A* and *B*) Representative images of two IHCs from SE WT (*A*) and ZnT3-KO (*B*) mice showing the baseline number of intact ribbons/IHC. (*C* and *D*) Representative hair cells from WT (*C*) and ZnT3-KO (*D*) mouse whole mounts 1 d after NE. (Scale bars: 10 μm.) (*E*) Quantification of the average intact ribbon synapses/IHC across cochlear frequencies (8, 12, 16, 24, and 32 kHz) in all groups (SE vs. NE, WT vs. ZnT3-KO) 1 d post-NE. Data in (*E*) are separated by genotype in (*F*). (*F*) Average intact ribbon synapses/IHC 1 d post-NE or -SE separated by genotype. WT mice (*Left*, black) have significantly reduced ribbons/IHC at high-frequency regions of the cochlea (24 to 32 kHz). ZnT3-KO mice (*Right*, red) do not have reduced ribbons/IHC at any measured cochlear region (*$P < 0.05$ for post hoc *t* test between SE and NE at specified frequency; n = 3/group). (*G*) Average intact ribbon synapses/IHC across cochlear frequencies (8, 12, 16, 24, and 32 kHz) in all groups (SE vs. NE, WT vs. ZnT3-KO) 14 d post-NE. Data in (*G*) are separated by genotype in (*H*). (*H*) Average intact ribbon synapses/IHC 14 d post-NE or -SE separated by genotype. WT mice (*Left*, black) have significantly reduced ribbons/IHC at high-frequency regions of the cochlea (24 to 32 kHz). ZnT3-KO mice (*Right*, red) do not have reduced ribbons/IHC at any measured cochlear region (*$P < 0.0001$ for post hoc *t* test between SE and NE at specified frequency; n NE = 5/genotype, SE = 3/genotype). Data are shown as mean ± SEM. For statistical details, see *SI Appendix*, Table S1.

synapses per IHC in WT mice in high-frequency areas of the cochlea (Fig. 6 *A*, *C*, *E*, and *F* black, note that the data in *E* are separated by genotype in *F*). In contrast, NE did not reduce the number of intact ribbon synapses in ZnT3-KO mice (Fig. 6 *B*, *D*, *E*, and *F* red), suggesting that *Slc30a3* gene deletion mitigates noise-induced synaptopathy.

To test whether the protection of ribbon synapses in ZnT3-KO mice persists after NE, we analyzed ribbon synapses 14 d after NE or SE. We found that in WT mice, the reduction in intact ribbon synapses persisted 14 d after NE (Fig. 6 *G* and *H*, black, note that the data in *G* are separated by genotype in *H*). In contrast, 14 d after NE, ZnT3-KO mice did not show a significant reduction in ribbon synapses (Fig. 6 *G* and *H*, red). These results indicate that elimination of ZnT3-dependent zinc signaling protects against ribbon synapse loss after NE and suggest that dysregulated labile zinc signaling likely contributes to NE-induced cochlear synaptopathy.

Zinc Chelation Mitigates NIHL. Constitutive ZnT3-KO mice lack ZnT3 from birth, which could impact the development of the cochlea and/or lead to changes in other signaling pathways that might affect the impact of ZnT3 deletion after NE. To determine whether the NIHL mitigation in ZnT3-KO mice is due to an acute lack of zinc signaling in adult mice, and to test whether zinc chelation protects against NIHL, we dissolved TPEN, a membrane-permeable high-affinity zinc chelator (58), in a hydrogel (poloxamer 407, Otonomy) to slowly deliver TPEN through the round window of the cochlea (see *Materials and Methods* for details). Two days before noise trauma, we surgically applied the hydrogel in mice, containing either TPEN (TPEN surgery ear) or vehicle (vehicle surgery ear). The contralateral ear was untreated and was used as a control for potential effects of surgery on hearing thresholds. Mice were allowed to recover for 2 d and then were bilaterally exposed to noise. We recorded ABRs and DPOAEs, before surgery, 2 d postsurgery but before NE, and again at 1 d and 14 d after NE (Fig. 7*A*). ABRs and DPOAEs were also measured from the contralateral ear, which did not receive surgery (vehicle control ear and TPEN control ear). We found that surgery resulted in a small but significant increase in ABR and DPOAE threshold shifts (*SI Appendix*, Fig. S6 *A* and *B*), but there was no significant difference between TPEN- and vehicle-treated mice after surgery (*SI Appendix*, Fig. S6 *A* and *B*), suggesting that surgical application of TPEN does not affect hearing thresholds shifts due to surgery.

We next assessed the effect of TPEN on ABR threshold shifts 1 d after NE. We found that the TPEN surgery ears had significantly lower ABR threshold shifts than vehicle surgery ears (Fig. 7*B*, three-way ANOVA). Note that we did not average across frequencies, as in Fig. 5, because we found a significant effect of frequency (*SI Appendix*, Table S1). These data suggest that surgical application of TPEN is protective against noise-induced ABR threshold shifts 1 d after NE. When ABRs were assessed 14 d post-NE, we found that TPEN surgery ears had reduced ABR threshold shifts compared to vehicle surgery ears (Fig. 7*C*), suggesting that this protection can last at least 14 d post-NE. We did not find any difference in the Wave IV/I ratio between vehicle- and TPEN-treated mice either at 1 d or 14 d after NE, suggesting that changes in brainstem gain in response to NE likely do not contribute to the enhanced protection of ABR threshold shifts by TPEN (*SI Appendix*, Fig. S6 *C* and *D*).

To assess OHC function in these mice, we next measured DPOAE threshold shifts at 1 d and 14 d after NE. In contrast to ABRs, DPOAE threshold shifts were not affected by local TPEN application 1 d post-NE (Fig. 7*D*). However, 14 d after NE DPOAE threshold shifts were smaller in the TPEN surgery ears compared to the vehicle

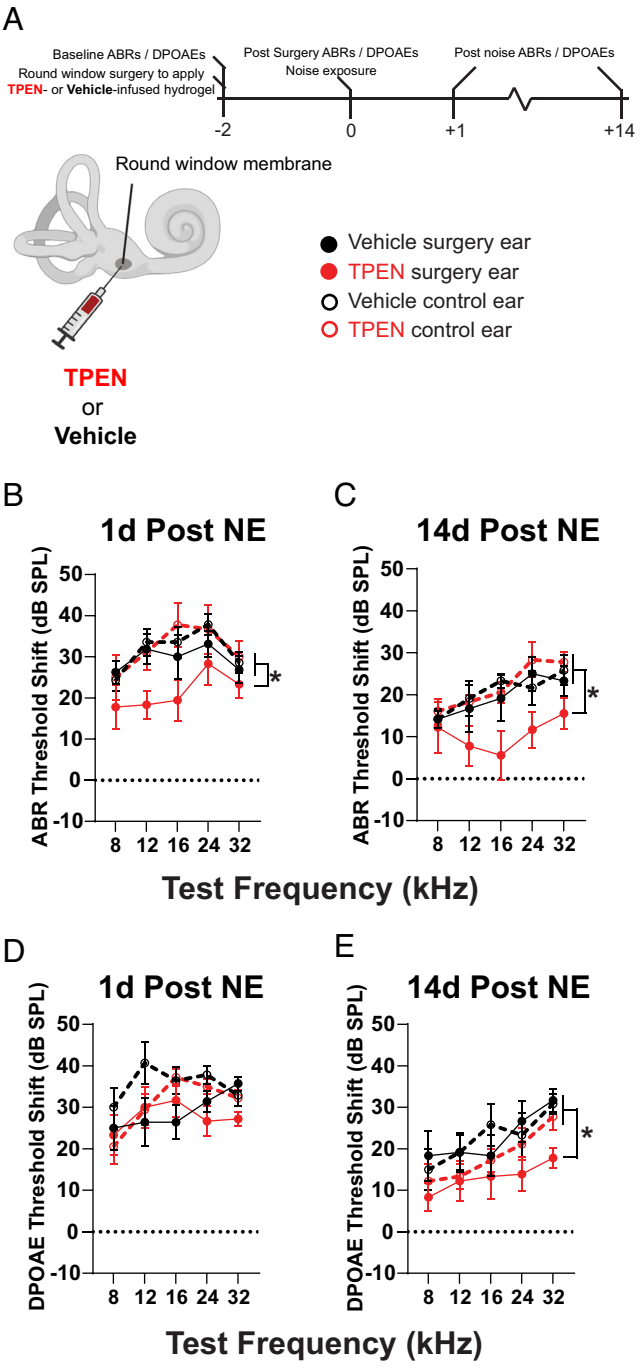

Fig. 7. Cochlear zinc chelation with TPEN prior to NE promotes protection and recovery of hair cell function after NE. (*A*) Experimental design of surgical application of TPEN or vehicle (5% ethanol in 1× PBS) in the cochlea via round window infusion. (*B*) ABR threshold shifts 1 d post-NE. Ears that received TPEN have smaller ABR threshold shifts than ears that received Vehicle and ears that did not receive surgery (Interaction Surgery × Drug Treatment: **P* = 0.0263; n = 8 Veh Surgery Ear, 9 TPEN Surgery Ear, 7 Veh Control Ear, 9 TPEN Control Ear). (*C*) ABR threshold shifts 14 d post-NE. Ears that received TPEN have smaller ABR threshold shifts than ears that received Vehicle and ears that did not receive surgery (Interaction Surgery × Drug **P* = 0.0059; n = 7 Veh Surgery Ear, 9 TPEN Surgery Ear, 7 Veh Control Ear, 9 TPEN Control Ear). (*D*) DPOAE threshold shifts 1 d post-NE. TPEN application did not affect DPOAE threshold shifts 1 d post-NE (Interaction Surgery × Drug Treatment *P* = 0.3013; n = 7 Veh Surgery Ear, 9 TPEN Surgery Ear, 7 Veh Control Ear, 9 TPEN Control Ear). (*E*) DPOAE threshold shifts 14 d post-NE. Ears that received TPEN have smaller DPOAE threshold shifts than ears that received Vehicle and ears that did not receive surgery (Interaction Surgery × Drug Treatment *P* = 0.0373; n = 7 Veh Surgery Ear, 9 TPEN Surgery Ear, 7 Veh Control Ear, 9 TPEN Control Ear). Data are shown as mean ± SEM. For statistical details, see *SI Appendix*, Table S1.

surgery ears (Fig. 7*E*). These results suggest that local chelation of zinc with TPEN enhances the recovery of OHC function after NE.

To control for the effects of surgical manipulation on zinc chelator-enhanced protection and recovery of hearing thresholds, we additionally evaluated post-NE ABRs and DPOAEs in control ears. At both 1 d after NE and 14 d after NE, we found that vehicle surgery ears were not significantly different from vehicle control ears in either ABR (Fig. 7 *B* and *C*) or DPOAE threshold shifts (Fig. 7 *D* and *E*), suggesting that the surgical intervention itself does not affect either the protection or recovery of hearing thresholds after noise trauma. Finally, control TPEN ears were not different from vehicle control ears suggesting that TPEN application does not affect either the protection or recovery of hearing thresholds in the contralateral after noise trauma (Fig. 7 *B–E*). Together, these results support that cochlear application of TPEN prior to noise trauma enhances the protection of overall peripheral function (ABRs at 1 d post-NE) and the recovery of OHC function (DPOAEs at 14 d post-NE) and thus mitigates NIHL.

To examine the effect of cochlear zinc chelation on synaptopathy, we performed cochlea histological evaluation in TPEN-treated mice. We found that round window TPEN treatment had no significant effect on noise-induced synaptopathy (*SI Appendix*, Fig. S6 *E–J*). These data are in contrast with ZnT3-KO mice, which showed protection against cochlear synaptopathy, suggesting that either the level of zinc chelation was not sufficient to protect against synaptopathy, or that *Slc30a3* gene germline deletion, leading to ZnT3 knockout, affects additional mechanisms compared to acute zinc signaling disruption in adult mice (*Discussion*).

To investigate whether systemic chelation of zinc signaling mitigates NIHL, we performed additional experiments in which we treated WT mice with intraperitoneal injection (i.p.) of TPEN (10 mg/kg) or vehicle (5 % ethanol in 0.9% saline) 3 h prior to, immediately after, and once a day for 4 d after SE or NE (*SI Appendix*, Fig. S7*A*). One day after NE, we found that ABR and DPOAE threshold shifts were not affected by systemic TPEN treatment, compared to vehicle treatment (*SI Appendix*, Fig. S7 *B*, *C*, *F*, and *G*). However, 14 d after NE, we found that TPEN-treated mice had lower ABR and DPOAE threshold shifts relative to vehicle-treated mice (*SI Appendix*, Fig. S7 *D*, *E*, *H*, and *I*), suggesting that a systemic reduction of zinc signaling in adult mice contributes to enhanced recovery of cochlear function after NE. We did not find any difference in the Wave IV/I ratio between vehicle- and TPEN-treated mice either at 1 d or 14 d after NE, suggesting that changes in brainstem gain in response to NE likely do not contribute to the enhanced recovery of cochlear function by systemic TPEN administration (*SI Appendix*, Fig. S8 *A* and *B*). As with cochlear zinc chelation, systemic zinc chelation had no significant effect on synaptopathy (*SI Appendix*, Fig. S8 *C–H*). To confirm that i.p. TPEN chelates cochlear zinc, we performed Timm staining in the cochlea from mice treated with TPEN or TPEN that was presaturated with zinc. We observed reduced zinc staining in the cochlea from mice treated with TPEN compared to the cochlea from mice treated with presaturated TPEN, indicating that i.p. TPEN treatment reduced the amount of labile zinc in the cochlea (*SI Appendix*, Fig. S8 *I–L*). Together, these data suggest that systemic application of TPEN has preventive therapeutic effects similar to surgical application in the cochlea. Importantly, these data support that either cochlear or systemic disruption of zinc signaling with a zinc chelator mitigate NIHL.

Discussion

Here, we demonstrated that labile zinc and ZnT3 are localized to specific subsets of cochlear cells; noise trauma induces dysregulation of cochlear zinc signaling; and disruption of zinc signaling mitigates NIHL. These results highlight zinc signaling as a potential target for preventing and mitigating NIHL.

Mechanisms of Zinc-Mediated Toxicity in the Cochlea. ZnT3-dependent increases in labile zinc contribute to neurodegeneration in models of optic nerve crush, seizures, and stroke (31, 59–61). Importantly, zinc chelation can limit the extent of neural damage and enhance recovery in these models (30–32). In particular, retinal ganglion cells display reduced cell death and increased axonal regrowth following zinc chelation (31, 32). Our results in the cochlea complement and expand on the importance of zinc chelation in preventing damage and enhancing recovery from trauma.

While our study supports the notion that either zinc chelation or ZnT3 knockout due to *Slc30a3* gene deletion enhance recovery of cochlear function after noise trauma and thus mitigate NIHL, it does not address either the mechanisms underlying cochlear damage or how zinc chelation mitigates this damage. In terms of mechanisms, the generation of reactive oxygen species (ROS) has been implicated in the pathology of NIHL (1, 62–65). Likewise, zinc homeostasis and deleterious zinc signaling are closely associated with the generation of ROS (66–69). While tight regulation of zinc signaling is critical for combating oxidative damage, zinc dysregulation is a prominent contributor to pathological signaling cascades that lead to increased ROS generation, such as NADPH oxidase and 12-LOX signaling pathways (66, 67). Abnormal zinc accumulation is also associated with mitochondrial dysfunction, which induces excessive ROS generation (70, 71). Moreover, ZnT3-KO mice and mice treated with zinc chelators show reduced ROS formation under conditions of hypoglycemia (72, 73), indicating that ZnT3-dependent zinc can contribute directly to oxidative stress under toxic conditions. Oxidative stress is also associated with increased ZnT3 dimerization/oligomerization and vesicular targeting (74). While we did not assess potential changes in the vesicular ZnT3 localization after noise trauma, our Western blot data support an increase in the 84 kDa ZnT3-immunoreactive band, which is consistent with increases ZnT3 dimerization (*SI Appendix*, Fig. S4 *B–D*), although we note that molecular weight equivalence to two putative ZnT3 monomers does not prove ZnT3 dimerization. Taken together, although we did not explore the mechanism of zinc-related pathology in this study, we propose that a noise-induced increase and dysregulation of labile zinc contributes to and/or interacts with excessive ROS generation in NIHL. Further studies simultaneously investigating molecular markers of oxidative stress, and ZnT3 and labile zinc dynamics will be critical to determine how they are linked in the context of NIHL.

Another common pathological mechanism linked to dysregulation of intracellular zinc is the zinc-dependent increased membrane insertion of Kv2.1 channels, which are important for regulating potassium flow out of hair cells (75). This abberant insertion of Kv2.1 channels leads to changes in potassium efflux and eventual apoptotic signaling (76). Although we did not observe any effects of cell death, hair cell loss often occurs later than 2 wk after acoustic trauma, even when hair cell function is impaired immediately after NE (77–79). As our studies were limited to 2 wk after noise trauma, our data cannot rule out the possibility of hair cell death that may occur later than 2 wk after noise-induced zinc dysregulation. Future experiments investigating molecular markers of degenerative signaling pathways, such as Kv2.1 membrane insertion, and the long-term effects of zinc dysregulation on cochlear histopathology may further elucidate the cytotoxic mechanisms that are activated by noise-induced zinc dysregulation.

Intracellular, Intercellular, and Extracellular Cochlear Zinc Dysregulation after Noise Trauma. Although our studies support the concept that ZnT3-dependent labile zinc is a critical contributor to the overall dysregulation of zinc signaling, zinc from other intracellular, intercellular, and extracellular sources likely contributes to zinc-dependent cochlear degeneration. At present, 24 zinc transporters (ZnTs and ZIPs) have been identified, which work in concert along with zinc-buffering metallothioneins (MTs) to tightly regulate the concentration and distribution of zinc. Zinc cannot be synthesized by cells, and yet we observe an increase in labile zinc following NE (Fig. 4). Most of the zinc in all cells is tightly bound to proteins and cannot be stained/detected with Timm staining, which only stains unbound (mobile) zinc (18, 46). However, cellular stress and other factors can cause liberation of protein-bound zinc from MTs and thus can lead to increased mobile zinc staining (dysregulation), without changes in total zinc levels (80, 81). Thus, the increase in labile zinc staining after noise trauma likely reflects an increase in unbound labile zinc not necessarily associated with changes in total zinc level. In this context, we view ZnT3-dependent zinc as a trigger for the initiation of zinc liberation/mobilization and subsequent mobile zinc dysregulation. In other areas, insult-induced zinc dysregulation can be ZnT3-dependent, as evidenced in the retina (31), or ZnT3-independent, as evidenced in the forebrain (82). In the cochlea, we propose that zinc dysregulation following noise trauma is induced by a ZnT3-dependent process, but it likely includes changes in additional other sources of intracellular zinc, as well.

Additionally, labile zinc can be mobilized between cells after noise trauma, as has been demonstrated in the retina following optic nerve crush (31). If intercellular mobilization of zinc does occur, one potential source for increased labile zinc in hair cells could be the SL fibrocytes. However, we do not know whether zinc released from SL fibrocytes can access the organ of Corti. Presumably, if zinc is released into the endolymph or onto SGN axons, it may diffuse and access hair cells and their synapses. However, in the retina, the time course of this intercellular mobilization requires multiple days, and up to 1 d after nerve crush, increases in labile zinc were primarily observed within the amacrine cells that already contained labile zinc. Therefore, although we cannot exclude intercellular mobilization of zinc, based on the time course of our results relative to other studies of intercellular zinc mobilization, we favor the hypothesis that, at 1 d post-NE, the increase in cochlear labile zinc signal is most likely of intracellular origin. Alternatively, it is possible that labile zinc reaches the hair cells via the tectorial membrane or extracellular zinc microdomains, spatial domains with high concentrations of unbound zinc (see next *Discussion* section) (83). Consistent with all these possibilities for zinc mobilization, all cochlear cell types express multiple ZnTs, ZIPs, and MTs (36, 38, 84) that can readily redistribute zinc intra- and intercellularly. Future experiments employing genetically encoded fluorescent zinc sensors (85) and extracellular zinc chelators, such as ZX1 or CaEDTA, will be necessary for further assessing the subcellular, cellular, and intercellular spatiotemporal zinc dynamics in the cochlea and the specific sources of zinc dysregulation after NE.

Potential Nonvesicular ZnT3 Localization and Function in the Cochlea. Our data demonstrate ZnT3 protein and labile zinc localization in the adult cochlea (Figs. 1–3). However, the function of ZnT3 and labile zinc in the normal cochlea function remains unknown. In the brain, ZnT3 is expressed in synaptic vesicles and ZnT3-dependent free zinc is released from axon terminals to modulate neurotransmission and sensory processing and adaptation (20–22, 26, 27, 86–88). In the cochlea, however, we observed ZnT3 (Fig. 2) and labile zinc (Fig. 3) in the stereocilia of OHCs, where there is no evidence for vesicles. One hypothesis for the role of stereocilia ZnT3 and zinc signaling is that it may function in a manner similar to ZnT1, another zinc transporter which functions to organize zinc into microdomains around NMDA receptors, thereby enabling zinc-mediated inhibition on NMDAR excitatory postsynaptic currents (83). In this context, it is tempting to speculate that ZnT3 may transport zinc from within the stereocilia to the outside of the cell, creating high concentrations of unbound zinc as observed in our Timm stains (Fig. 3), where zinc may modulate the function of ion channels or transporters, including the hair cell stereocilia mechanotransduction (MET) channel complex or PMCA2 calcium pumps. Moreover, Piezo2 channels, which are mechanically sensitive ion channels located on the apical cell body of OHCs (89), distinct from the stereocilia MET channel, are another potential target of zinc signaling. Piezo1 channels have a very similar structure to Piezo2 channels (90, 91); and zinc, but not calcium or magnesium, decreases Piezo1 channel inactivation (92). The exact function of Piezo2 channels in the cochlea is not yet fully understood, although these channels conduct reverse-polarity currents in response to stereocilia deflection in directions opposite to the stereocilia MET channel (89). Reverse-polarity currents are thought to be involved in regulating the maturation of and continuous repair of the MET sensory transduction machinery (89, 93–95). Thus, zincergic modulation of these channels might be important for regulating the development of sensory hair cell transduction machinery and/or hair cell repair processes following injury. The nonvesicular localization of ZnT3 in the stereocilia might signify a modulatory role of zinc on the MET machinery in OHCs.

Alternatively, zinc maybe localized to another structure apposed to the stereocilia, such as the tectorial membrane that is in contact with the stereocilia. This is consistent with our results on zinc localization in the stereocilia of OHCs but not IHCs and the fact that the tectorial membrane makes physical contact with the OHC but not with the IHC stereocilia (96). Furthermore, there is precedent for the tectorial membrane acting as a source for ions that impact stereocilia. The tectorial membrane can act as a source for Ca^{2+} that affects hair cell function (97). Notably, this Ca^{2+} source is impacted with noise exposure. Additionally, the tectorial membrane is attached to the SL, which contains zinc and ZnT3-expressing cells (Figs. 1–3). Regardless, future high-resolution localization electron microscopy studies are needed to clearly determine the precise subcellular localization of ZnT3 and labile zinc in conjunction with physiological experiments investigating the normal function of zinc signaling in hair cells are necessary.

Differences in the Protection and Recovery Profiles of Zinc Removal Methods. In our study, we defined "protection" as a significant improvement in ABRs or DPOAEs 1 d after NE (e.g., Figs. 5*F* and 7*B*), and "recovery" as a significant improvement at 14 d after NE, especially if no effect was observed 1 d after NE (e.g., Figs. 5*E* and 7*E*). However, one limitation of this interpretation is that we cannot assess with certainty whether differences in hearing thresholds at these time points reflect protection against or recovery from NE. Specifically, our experiments cannot distinguish whether an effect observed 1 d after NE is the result of a rapid recovery process that begins at an earlier time point after NE. Furthermore, our experiments cannot determine whether an effect observed at 14 d after NE reflects an enhanced recovery process following similar initial damage or whether improved hearing thresholds at 14 d are a consequence of a protective effect that occurred at an earlier time. To confidently assess the differences between

protection and recovery, subsequent experiments using additional time points and the evaluation of distinct molecular signaling pathways following NE will be required. Nonetheless, our studies clearly establish zinc signaling as a major player in noise-induced degeneration and subsequent partial recovery in the cochlea.

In all experiments, zinc signaling was disrupted prior to NE. Therefore, although our experiments do not test a potential therapeutic effect of zinc signaling disruption after NE, they support a prophylactic approach to mitigate NIHL. Future experiments where chelators are administered after NE will be needed to determine the therapeutic window for zinc chelation after NE.

We chose TPEN, which is as a high-affinity and membrane-permeable zinc chelator (58), to maximize the likelihood of entry and zinc chelation in the cochlea. A limitation of TPEN, however, is that it also binds copper and other transition metals with high affinity (58), although the available amounts of chelatable forms of copper are negligibly small within cells (98). Importantly, the overall similar effects observed between ZnT3-KO mice and TPEN-treated mice support the notion that zinc is the relevant metal that is disrupted by TPEN in our experiments.

Although the overall profile of NIHL mitigation is similar between ZnT3-KO and TPEN-treated mice, we observed some differences between the two methods of zinc disruption. We noted differences in ABR threshold shifts, DPOAE threshold shifts, and synaptopathy at 1 d and/or 14 d post-NE (Figs. 5–7 and *SI Appendix*, Fig. S7). Namely, we observed that ZnT3-KO mice exhibit enhanced protection against both DPOAE threshold shifts (Fig. 5 *F* and *G*) and synaptopathy (Fig. 6) 1 d after NE. Conversely, mice treated with local or systemic TPEN show recovery of DPOAE threshold shifts 14 d after NE (Fig. 7 *D* and *E* and *SI Appendix*, Fig. S7 *F–I*) and no protection or recovery against synaptopathy (*SI Appendix*, Figs. S6 and S8). It is possible that our methods, dosages, and/or time points of TPEN delivery are suboptimal, but these differences may also suggest that the pathological mechanisms that underlie noise-induced OHC damage and synaptopathy may be specifically dependent on ZnT3-dependent zinc. Another explanation is that constitutive disruption of ZnT3-dependent zinc signaling in ZnT3-KO mice may lead to secondary developmental differences due to the absence of ZnT3, which could underlie the protective effects of ZnT3 knockout due to *Slc30a3* gene deletion on OHC function and synaptopathy. This hypothesis will be addressed in future studies using the recently characterized ZnT3-CreER^{T2}/Rox mouse-line (34), which would allow for inducible ZnT3-KO in the cochlea in adulthood, therefore bypassing developmental confounds.

We also observed that cochlear zinc chelation with TPEN enhances protection against ABR threshold shifts 1 d after NE (Fig. 7), whereas ZnT3 knockout due to *Slc30a3* gene deletion only enhanced recovery of ABR threshold shifts 14 d after NE (Fig. 5). This difference suggests that overall protection of cochlear function after NE is not solely dependent on ZnT3-dependent zinc. Rather, it suggests that in addition to ZnT3-dependent zinc, noise-induced cochlear degeneration involves dysregulated zinc liberated from other cellular sources (e.g., metallothioneins) that can be affected by local zinc chelation. Additionally, systemic zinc chelation (*SI Appendix*, Fig. S7) was not as effective as local zinc chelation (Fig. 7) at protecting against ABR threshold shifts 1 d after NE. We did not compare the concentration of TPEN in the cochlea after each delivery method, but one explanation for this difference is that the different routes of drug administration result in different drug concentrations and thus zinc chelation in the cochlea. Moreover, untested methods of administration, such as posterior semicircular canal injection, could yield stronger protection and recovery than observed in our studies.

Materials and Methods

Male mice, P42–P61, were used for all experiments. All animal procedures were approved by Institutional Animal Care and Use Committees of the University of Pittsburgh. To cause cochlear damage and hearing loss, we bilaterally exposed unanesthetized mice to 100 dB SPL 8 to 16 kHz noise for 2 h. To assess zinc signaling in the healthy and damaged cochlea, we used transgenic mice, immunohistochemistry, and zinc autometallography. Cochlear structural damage and recovery were assessed with fluorescent immunohistochemistry. Cochlear function and hearing damage and recovery were assessed with auditory brainstem response (ABR) and distortion product otoacoustic emission (DPOAE) measurements. Finally, to test the effect of zinc chelation on cochlear damage and hearing loss, we applied the membrane-permeable zinc chelator, TPEN, through the round window of the cochlea or with intraperitoneal injection. Details on methods, data analysis, and statistics are provided in *SI Appendix, Materials and Methods*.

Data, Materials, and Software Availability. Datasets used in figures are posted publicly on Figshare (99). All other data are included in the article and/or *SI Appendix*.

ACKNOWLEDGMENTS. We thank Otonomy for their generous donation of Poloxamer 408 used in our surgical experiments. The ZnT3-HA mice were generated with the Innovative Technologies Development Core at the University of Pittsburgh. This work was supported by NIH grants R01-DC020923, R01-DC019618, R01-EB033172 (T.T.), F31-DC019027 (B.B.), R01-AG058851 (A.T.), and R21-DC019195 (C.L.C.).

1. A. Kurabi *et al.*, Cellular mechanisms of noise-induced hearing loss. *Hear Res.* **349**, 129–137 (2017).
2. National Institute on Deafness and Other Communication Disorders, Quick Statistics (2021). https://www.nidcd.nih.gov/health/statistics/quick-statistics-hearing. Accessed 31 March 2022.
3. National Institute on Deafness and Other Communication Disorders, Noise Induced Hearing Loss (2007). https://www.nidcd.nih.gov/health/noise-induced-hearing-loss. Accessed 31 March 2022.
4. World Health Organization, Deafness and Hearing Loss (2023). https://www.who.int/en/news-room/fact-sheets/detail/deafness-and-hearing-loss. Accessed 31 March 2022.
5. G. B. D. H. L. Collaborators, Hearing loss prevalence and years lived with disability, 1990–2019: Findings from the Global Burden of Disease Study 2019. *Lancet* **397**, 996–1009 (2021).
6. S. I. Cho *et al.*, Mechanisms of hearing loss after blast injury to the ear. *PLoS One* **8**, e67618 (2013).
7. J. H. Patterson Jr., R. P. Hamernik, Blast overpressure induced structural and functional changes in the auditory system. *Toxicology* **121**, 29–40 (1997).
8. Y. Wang, K. Hirose, M. C. Liberman, Dynamics of noise-induced cellular injury and repair in the mouse cochlea. *J. Assoc. Res. Otolaryngol.* **3**, 248–268 (2002).
9. S. G. Kujawa, M. C. Liberman, Adding insult to injury: Cochlear nerve degeneration after "temporary" noise-induced hearing loss. *J. Neurosci.* **29**, 14077–14085 (2009).
10. L. D. Liberman, H. Wang, M. C. Liberman, Opposing gradients of ribbon size and AMPA receptor expression underlie sensitivity differences among cochlear-nerve/hair-cell synapses. *J. Neurosci.* **31**, 801–808 (2011).
11. C. J. Plack, D. Barker, G. Prendergast, Perceptual consequences of "hidden" hearing loss. *Trends Hear.* **18**, 2331216514550621 (2014).
12. C. Andreini *et al.*, Counting the zinc-proteins encoded in the human genome. *J. Proteome Res.* **5**, 196–201 (2006).
13. A. S. Nakashima, R. H. Dyck, Zinc and cortical plasticity. *Brain Res. Rev.* **59**, 347–373 (2009).
14. C. J. Frederickson, Neurobiology of zinc and zinc-containing neurons. *Int. Rev. Neurobiol.* **31**, 145–238 (1989).
15. C. J. Frederickson, J. Y. Koh, A. I. Bush, The neurobiology of zinc in health and disease. *Nat. Rev. Neurosci.* **6**, 449–462 (2005).
16. W. Maret, Zinc in the biosciences. *Metallomics* **6**, 1174 (2014).
17. R. D. Palmiter *et al.*, ZnT-3, a putative transporter of zinc into synaptic vesicles. *Proc. Natl. Acad. Sci. U.S.A.* **93**, 14934–14939 (1996).
18. T. B. Cole *et al.*, Elimination of zinc from synaptic vesicles in the intact mouse brain by disruption of the ZnT3 gene. *Proc. Natl. Acad. Sci. U.S.A.* **96**, 1716–1721 (1999).
19. N. Upmanyu *et al.*, Colocalization of different neurotransmitter transporters on synaptic vesicles is sparse except for VGLUT1 and ZnT3. *Neuron* **110**, 1483–1497.e7 (2022).
20. C. T. Anderson *et al.*, Cell-specific gain modulation by synaptically released zinc in cortical circuits of audition. *Elife* **6**, e29893 (2017).
21. M. Kumar *et al.*, Fine control of sound frequency tuning and frequency discrimination acuity by synaptic zinc signaling in mouse auditory cortex. *J. Neurosci.* **39**, 854–865 (2019).
22. P. A. Cody, T. Tzounopoulos, Neuromodulatory mechanisms underlying contrast gain control in mouse auditory cortex. *J. Neurosci.* **42**, 5564–5579 (2022).
23. C. E. Brown, R. H. Dyck, Rapid, experience-dependent changes in levels of synaptic zinc in primary somatosensory cortex of the adult mouse. *J. Neurosci.* **22**, 2617–2625 (2002).
24. T. Perez-Rosello *et al.*, Tonic zinc inhibits spontaneous firing in dorsal cochlear nucleus principal neurons by enhancing glycinergic neurotransmission. *Neurobiol. Dis.* **81**, 14–19 (2015).

25. S. Kouvaros, M. Kumar, T. Tzounopoulos, Synaptic zinc enhances inhibition mediated by somatostatin, but not parvalbumin, cells in mouse auditory cortex. *Cereb Cortex* **30**, 3895–3909 (2020).
26. C. T. Anderson *et al.*, Modulation of extrasynaptic NMDA receptors by synaptic and tonic zinc. *Proc. Natl. Acad. Sci. U.S.A.* **112**, E2705–E2714 (2015).
27. N. W. Vogler *et al.*, Mechanisms underlying long-term synaptic zinc plasticity at mouse dorsal cochlear nucleus glutamatergic synapses. *J. Neurosci.* **40**, 4981–4996 (2020).
28. B. I. Kalappa *et al.*, AMPA receptor inhibition by synaptically released zinc. *Proc. Natl. Acad. Sci. U.S.A.* **112**, 15749–15754 (2015).
29. S. L. Galasso, R. H. Dyck, The role of zinc in cerebral ischemia. *Mol. Med.* **13**, 380–387 (2007).
30. Y. Zhao *et al.*, Chelating intracellularly accumulated zinc decreased ischemic brain injury through reducing neuronal apoptotic death. *Stroke* **45**, 1139–1147 (2014).
31. Y. Li *et al.*, Mobile zinc increases rapidly in the retina after optic nerve injury and regulates ganglion cell survival and optic nerve regeneration. *Proc. Natl. Acad. Sci. U.S.A.* **114**, E209–E218 (2017).
32. E. F. Trakhtenberg *et al.*, Zinc chelation and Klf9 knockdown cooperatively promote axon regeneration after optic nerve injury. *Exp. Neurol.* **300**, 22–29 (2018).
33. G. E. Shambaugh Jr., Zinc and presbycusis. *Am. J. Otol.* **6**, 116–117 (1985).
34. S. Kouvaros *et al.*, A CRE/DRE dual recombinase transgenic mouse reveals synaptic zinc-mediated thalamocortical neuromodulation. *Sci. Adv.* **9**, eadf3525 (2023).
35. Z. Su *et al.*, LncRNA AW112010 promotes mitochondrial biogenesis and hair cell survival: Implications for age-related hearing loss. *Oxid Med. Cell Longev.* **2019**, 6150148 (2019).
36. B. Milon *et al.*, A cell-type-specific atlas of the inner ear transcriptional response to acoustic trauma. *Cell Rep.* **36**, 109758 (2021).
37. H. Liu *et al.*, Characterization of transcriptomes of cochlear inner and outer hair cells. *J. Neurosci.* **34**, 11085–11095 (2014).
38. Y. Li *et al.*, Transcriptomes of cochlear inner and outer hair cells from adult mice. *Sci. Data* **5**, 180199 (2018).
39. N. Peeleman *et al.*, On the role of fibrocytes and the extracellular matrix in the physiology and pathophysiology of the spiral ligament. *Front. Neurol.* **11**, 580639 (2020).
40. J. C. Adams, M. C. Liberman, "Anatomy" in Schuknecht's Pathology of the Ear, 3rd edition, 2010. S. N. Merchant, J. B. Nadol, Eds. (People's Medical Pub House-USA, 2010), pp. 75–76.
41. B. A. Nayagam, M. A. Muniak, D. K. Ryugo, The spiral ganglion: Connecting the peripheral and central auditory systems. *Hear Res.* **278**, 2–20 (2011).
42. H. Jiang *et al.*, Microvascular networks in the area of the auditory peripheral nervous system. *Hear Res.* **371**, 105–116 (2019).
43. L. Chessum *et al.*, Helios is a key transcriptional regulator of outer hair cell maturation. *Nature* **563**, 696–700 (2018).
44. C. E. Brown, R. H. Dyck, Distribution of zincergic neurons in the mouse forebrain. *J. Comp. Neurol.* **479**, 156–167 (2004).
45. H. J. Wenzel *et al.*, Ultrastructural localization of zinc transporter-3 (ZnT-3) to synaptic vesicle membranes within mossy fiber boutons in the hippocampus of mouse and monkey. *Proc. Natl. Acad. Sci. U.S.A.* **94**, 12676–12681 (1997).
46. G. Danscher, M. Stoltenberg, Zinc-specific autometallographic in vivo selenium methods: Tracing of zinc-enriched (ZEN) terminals, ZEN pathways, and pools of zinc ions in a multitude of other ZEN cells. *J. Histochem. Cytochem.* **53**, 141–153 (2005).
47. J. S. Buchwald, C. Huang, Far-field acoustic response: Origins in the cat. *Science* **189**, 382–384 (1975).
48. N. Y. Kiang, M. C. Liberman, R. A. Levine, Auditory-nerve activity in cats exposed to ototoxic drugs and high-intensity sounds. *Ann. Otol. Rhinol. Laryngol.* **85**, 752–768 (1976).
49. M. M. El-Badry, S. L. McFadden, Electrophysiological correlates of progressive sensorineural pathology in carboplatin-treated chinchillas. *Brain Res.* **1134**, 122–130 (2007).
50. G. A. Caprara, A. W. Peng, Mechanotransduction in mammalian sensory hair cells. *Mol. Cell Neurosci.* **120**, 103706 (2022).
51. G. Salazar *et al.*, The zinc transporter ZnT3 interacts with AP-3 and it is preferentially targeted to a distinct synaptic vesicle subpopulation. *Mol. Biol. Cell* **15**, 575–587 (2004).
52. H. Shen *et al.*, Zinc distribution and expression pattern of ZnT3 in mouse brain. *Biol. Trace Elem. Res.* **119**, 166–174 (2007).
53. S. G. Kujawa, M. C. Liberman, Acceleration of age-related hearing loss by early noise exposure: Evidence of a misspent youth. *J. Neurosci.* **26**, 2115–2123 (2006).
54. H. S. Li, Influence of genotype and age on acute acoustic trauma and recovery in CBA/Ca and C57BL/6J mice. *Acta Otolaryngol.* **112**, 956–967 (1992).
55. R. Probst, B. L. Lonsbury-Martin, G. K. Martin, A review of otoacoustic emissions. *J. Acoust. Soc. Am.* **89**, 2027–2067 (1991).
56. P. Avan *et al.*, Physiopathological significance of distortion-product otoacoustic emissions at 2f1-f2 produced by high- versus low-level stimuli. *J. Acoust. Soc. Am.* **113**, 430–441 (2003).
57. H. Spoendlin, Innervation densities of the cochlea. *Acta Otolaryngol.* **73**, 235–248 (1972).
58. R. J. Radford, S. J. Lippard, Chelators for investigating zinc metalloneurochemistry. *Curr. Opin. Chem. Biol.* **17**, 129–136 (2013).
59. J. Y. Koh *et al.*, The role of zinc in selective neuronal death after transient global cerebral ischemia. *Science* **272**, 1013–1016 (1996).
60. C. J. Frederickson, M. D. Hernandez, J. F. McGinty, Translocation of zinc may contribute to seizure-induced death of neurons. *Brain Res.* **480**, 317–321 (1989).
61. J. H. Weiss *et al.*, AMPA receptor activation potentiates zinc neurotoxicity. *Neuron* **10**, 43–49 (1993).
62. A. R. Fetoni *et al.*, Targeting dysregulation of redox homeostasis in noise-induced hearing loss: Oxidative stress and ROS signaling. *Free Radic. Biol. Med.* **135**, 46–59 (2019).
63. F. Wu, H. Xiong, S. Sha, Noise-induced loss of sensory hair cells is mediated by ROS/AMPKalpha pathway. *Redox Biol.* **29**, 101406 (2020).
64. M. Kishimoto-Urata *et al.*, Role of oxidative stress and antioxidants in acquired inner ear disorders. *Antioxidants (Basel)* **11**, 1469 (2022).
65. D. Yamashita *et al.*, Delayed production of free radicals following noise exposure. *Brain Res.* **1019**, 201–209 (2004).
66. K. M. Noh, J. Y. Koh, Induction and activation by zinc of NADPH oxidase in cultured cortical neurons and astrocytes. *J. Neurosci.* **20**, RC111 (2000).
67. Y. Zhang *et al.*, Peroxynitrite-induced neuronal apoptosis is mediated by intracellular zinc release and 12-lipoxygenase activation. *J. Neurosci.* **24**, 10616–10627 (2004).
68. E. Aizenman *et al.*, Complex role of zinc in methamphetamine toxicity in vitro. *Neuroscience* **171**, 31–39 (2010).
69. D. D. Marreiro *et al.*, Zinc and oxidative stress: Current mechanisms. *Antioxidants (Basel)* **6**, 24 (2017).
70. K. E. Dineley *et al.*, Zinc causes loss of membrane potential and elevates reactive oxygen species in rat brain mitochondria. *Mitochondrion* **5**, 55–65 (2005).
71. Y. V. Medvedeva, J. H. Weiss, Intramitochondrial Zn2+ accumulation via the Ca2+ uniporter contributes to acute ischemic neurodegeneration. *Neurobiol. Dis.* **68**, 137–144 (2014).
72. S. W. Suh *et al.*, Zinc release contributes to hypoglycemia-induced neuronal death. *Neurobiol. Dis.* **16**, 538–545 (2004).
73. S. W. Suh *et al.*, Sequential release of nitric oxide, zinc, and superoxide in hypoglycemic neuronal death. *J. Cereb. Blood Flow. Metab.* **28**, 1697–1706 (2008).
74. G. Salazar *et al.*, SLC30A3 (ZnT3) oligomerization by dityrosine bonds regulates its subcellular localization and metal transport capacity. *PLoS One* **4**, e5896 (2009).
75. X. Li *et al.*, Extracellular chloride regulation of Kv2.1, contributor to the major outward Kv current in mammalian outer hair cells. *Am. J. Physiol. Cell Physiol.* **302**, C296–C306 (2012).
76. P. T. Redman *et al.*, Regulation of apoptotic potassium currents by coordinated zinc-dependent signalling. *J. Physiol.* **587**, 4393–4404 (2009).
77. W. P. Yang *et al.*, Quantitative analysis of apoptotic and necrotic outer hair cells after exposure to different levels of continuous noise. *Hear Res.* **196**, 69–76 (2004).
78. R. P. Hamernik *et al.*, Anatomical correlates of impulse noise-induced mechanical damage in the cochlea. *Hear Res.* **13**, 229–247 (1984).
79. B. H. Hu, D. Henderson, T. M. Nicotera, Involvement of apoptosis in progression of cochlear lesion following exposure to intense noise. *Hear Res.* **166**, 62–71 (2002).
80. S. J. Lee, J. Y. Koh, Roles of zinc and metallothionein-3 in oxidative stress-induced lysosomal dysfunction, cell death, and autophagy in neurons and astrocytes. *Mol. Brain* **3**, 30 (2010).
81. W. Maret, A. Krezel, Cellular zinc and redox buffering capacity of metallothionein/thionein in health and disease. *Mol. Med.* **13**, 371–375 (2007).
82. J. Y. Lee *et al.*, Accumulation of zinc in degenerating hippocampal neurons of ZnT3-null mice after seizures: Evidence against synaptic vesicle origin. *J. Neurosci.* **20**, RC79 (2000).
83. R. F. Krall *et al.*, Synaptic zinc inhibition of NMDA receptors depends on the association of GluN2A with the zinc transporter ZnT1. *Sci. Adv.* **6**, eabb1515 (2020).
84. R. Hertzano *et al.*, Cell type-specific expression analysis of the inner ear: A technical report. *Laryngoscope* **131**, S1–S16 (2021).
85. T. Wu *et al.*, A genetically encoded far-red fluorescent indicator for imaging synaptically released Zn(2). *Sci. Adv.* **9**, eadd2058 (2023).
86. B. I. Kalappa, T. Tzounopoulos, Context-dependent modulation of excitatory synaptic strength by synaptically released zinc. *eNeuro* **4**, 0011–0017 (2017).
87. H. P. Patrick Wu, R. H. Dyck, Signaling by synaptic zinc is required for whisker-mediated, fine texture discrimination. *Neuroscience* **369**, 242–247 (2018).
88. A. Morabito *et al.*, Activity-dependent modulation of NMDA receptors by endogenous zinc shapes dendritic function in cortical neurons. *Cell Rep.* **38**, 110415 (2022).
89. Z. Wu *et al.*, Mechanosensory hair cells express two molecularly distinct mechanotransduction channels. *Nat. Neurosci.* **20**, 24–33 (2017).
90. F. J. Taberner *et al.*, Structure-guided examination of the mechanogating mechanism of PIEZO2. *Proc. Natl. Acad. Sci. U.S.A.* **116**, 14260–14269 (2019).
91. L. Wang *et al.*, Structure and mechanogating of the mammalian tactile channel PIEZO2. *Nature* **573**, 225–229 (2019).
92. P. A. Gottlieb, C. Bae, F. Sachs, Gating the mechanical channel Piezo1: A comparison between whole-cell and patch recording. *Channels (Austin)* **6**, 282–289 (2012).
93. K. X. Kim *et al.*, The role of transmembrane channel-like proteins in the operation of hair cell mechanotransducer channels. *J. Gen. Physiol.* **142**, 493–505 (2013).
94. W. Marcotti *et al.*, Transduction without tip links in cochlear hair cells is mediated by ion channels with permeation properties distinct from those of the mechano-electrical transducer channel. *J. Neurosci.* **34**, 5505–5514 (2014).
95. J. Waguespack *et al.*, Stepwise morphological and functional maturation of mechanotransduction in rat outer hair cells. *J. Neurosci.* **27**, 13890–13902 (2007).
96. I. J. Russell *et al.*, Sharpened cochlear tuning in a mouse with a genetically modified tectorial membrane. *Nat. Neurosci.* **10**, 215–223 (2007).
97. C. E. Strimbu *et al.*, Control of hearing sensitivity by tectorial membrane calcium. *Proc. Natl. Acad. Sci. U.S.A.* **116**, 5756–5764 (2019).
98. T. D. Rae *et al.*, Undetectable intracellular free copper: The requirement of a copper chaperone for superoxide dismutase. *Science* **284**, 805–808 (1999).
99. T. Tzounopoulos, B. Bizup, Cochlear zinc signaling dysregulation is associated with noise-induced hearing loss, and zinc chelation enhances cochlear recovery. Figshare. https://figshare.com/articles/dataset/Cochlear_zinc_signaling_dysregulation_is_associated_with_noise-induced_hearing_loss_and_zinc_chelation_enhances_cochlear_recovery/25093736. Deposited 27 January 2024.